Development of an Analytic Model for Flux Switching Motors

Mohammad Mardaneh[i] ; Mojtaba Mirsalim[ii]

ABSTRACT

This paper presents developing an analytical model for flux switching motors. The motor is a class of variable reluctance motors that has two windings on stator; a field winding and an armature winding. Due to saliency of both stator and rotor poles, accurate modeling is difficult which arises from the nonlinear behavior of the machine. This paper presents a simple model which is able to predict the motor inductances. The advantage of this method is that it describes the parameters of motor based on its dimensions. The model predicts both the self and mutual inductances. In comparison with similar studies, the proposed model predicts the mutual-inductance of a flux switching motor very accurately. It should be noted that the mutual-inductance has not previously been considered by others in their analytic modeling of variable reluctance motors. The predicted results computed by the proposed analytic model are compared to that obtained by the two-dimensional finite element analysis.

KEYWORDS

Analytical model, Flux witching motor, self- and mutual- inductances.

Symbols:

$N_{F/A}$: Number of field/armature winding turns

$\alpha_{s/r}$: Stator/rotor pole arc

l : Mean length of flux path in iron

g : Air gap length

l_{stk} : Stack length of machine

$l_{s/r}$: Length of stator/rotor slot

R_g : Mean radius in air gap

P_s : Number of stator poles

$g_{f1/2}$: The length of fringing flux path in air, position 1/2

a_s : Area of rotor-stator pole overlap

$a_{g1/2}$: Area of fringing flux component

a_m : Effective area to compute mutual inductance

T : Torque

$i_{F/A}$: Field/armature current

$L_{F/A}$: Field/armature self-inductance

L_{AF} : Mutual inductance between field and armature windings

θ : Rotor angle (degrees)

$H_{Fe,m}$: Main quantity of magnetic field intensity in iron

$H_{g,m}$: Main quantity of magnetic field intensity in air

$H_{Fe,f1/2}$: Fringing quantities of magnetic field intensity in iron

$H_{g,f1/2}$: Fringing quantities of magnetic field intensity in air

B_m : Main quantity of field

B_f : Fringing quantity of field

λ_{mF} : The main flux contribution to the total flux linked by the field winding

λ_{fF} : The fringing flux contribution to the total flux linked by the field winding

μ_0 : Permeability of free space

μ_r : Relative permeability of core

μ : Permeability of core

A : Vector potential

J : Current density

L_0 : Inductance at unaligned position

1. INTRODUCTION

The flux switching motor (FSM) is a new class of electrical motors which was introduced by C. Pollock [1] in 1999 and is gradually emerging in power tools and household applications. It is a combination of the switched reluctance motor (SRM) and the inductor alternator [1]. Figure 1 shows a physical construction of a FSM. The lamination profile is very similar to that of a two-phase 4/2 switched reluctance motor, thus allowing its simple construction and inherent robustness to be

[i] M. Mardaneh and M. Mirsalim *(IEEE Senior Member)* are with the Department of Electrical Engineering, Amirkabir University of Technology, Tehran, Iran (Email: m_mardaneh@aut.ac.ir).

[ii] M. Mirsalim is also with the Department of Electrical Engineering, San Antonio, TX, 78228 (e-mail: mmirsalim@stmarytx.edu).

retained. Stator and rotor poles are both salient. FSM has two full-pitched windings located in opposite slots of stator. One winding is constantly excited with a unipolar current which is named field winding (F), whilst the other, named armature winding (A), should be supplied with a bipolar current.

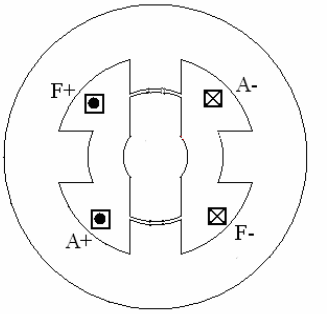

Figure 1: Physical construction of a FSM

The principle of operation of FSMs is based on the variation of the reluctance such as in SRMs, and has been described in the literature [1- 4].

While reluctance machines have the simplest construction among the electrical machines, their modeling, simulation, and design are less straight forward. The saliency of poles, saturation of lamination in aligned position of rotor and localized saturation in pole tips make some difficulties in modeling of reluctance motors. In comparison with other electric motors such as disc type motors [5-6] or permanent magnet machines [7] developing an analytical model for SRMs is more complicated. One encounters similar difficulties in the modeling of FSMs.

Numerous authors have attempted to model SRMs [8-9]. In a nutshell, the various methods of modeling SRMs in the literature are: flux-mmf-position or flux linkage-current-position surfaces [3], mathematical modeling and curve fitting techniques [10], analytical approaches [11, 12], magnetic circuit models [13], artificial intelligent methods [14], and finite element analysis. Each of those has its advantages and drawbacks [10-14].

The analytical modeling has the advantage of describing the motor parameters based on the geometry of machine. Radon [11] has developed an analytical model for SRMs. Two common assumptions in modeling of SRMs are: independence of flux linkages of phases, and negligible mutual inductance between phases. The latter assumption is incorrect in the case of high-speed operations where the current-overlap of phases is considerable or in the case of full-pitched windings of FSMs.

Pollock et al. have presented a simple model [1] and a dynamic simulation model [3] for FSMs. The former is not an accurate model and the latter needs pre-processing calculations by finite element analysis (FEA).

In this paper, an analytical approach to model FSM is presented. The advantage of this method is that it describes the parameters of motor based on its dimensions. The model predicts both the self and mutual inductances. In comparison with similar studies, the proposed model predicts the mutual-inductance of a flux switching motor very accurately. It should be noted that the mutual-inductance has not previously been considered by others in their analytic modeling of variable reluctance motors. This model can be easily applied in controlling or designing FSMs.

In the following sections, the idealized winding inductances are presented and then, an analytic model is introduced and the relevant relations are derived. Finally, the predicted results computed by the proposed analytic model are compared to that obtained by the two-dimensional finite element analysis.

2. SELF- AND MUTUAL INDUCTANCE PROFILES OF AN IDEAL WINDING

In this section it is assumed that the ideal inductances shown in figure 2 vary linearly with rotor position. As the rotor moves away from aligned position, the self inductances of field winding (F) and armature winding (A) decrease linearly to a minimum value due to the increase of reluctance. Because of similar path for the flux of F and A both windings have the same inductance profiles.

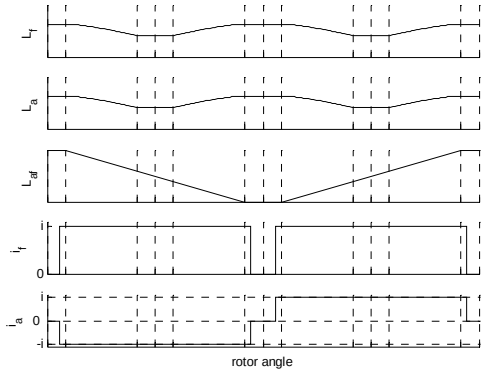

Figure 2: Idealized winding inductances and current waveforms

When the self inductance reaches its minimum value, it remains fairly constant. With further rotation of the rotor, the self inductances increase linearly since the rotor poles are approaching alignment with the stator poles. The mutual inductance between the armature and the field windings decreases linearly from its maximum positive value as the rotor moves away from the aligned position to the position where the rotor poles are between adjacent stator poles. The value of the mutual inductance at this location is equal to zero. As the rotor continues to rotate toward the next alignment position, the resultant flux will switch between the poles linked by field winding, and thus the mutual inductance becomes negative. The value

of mutual inductance will decrease to its minimum negative value at the end of half cycle. Similarly, for the other half cycle, the mutual inductance increases linearly to its maximum positive value at the end of the cycle, as shown in figure 3.

For positive torque production, the corresponding idealized winding currents are to be controlled, see figure 2. Note that the zero-current intervals, between the positive and negative armature current are purposely provided to ensure successful current reversal. Meanwhile, as two windings are in series, during the zero-current interval of armature current, the idealized field-winding current will consequently decay to zero, it may be consequent fewer losses. The developed torque is given by:

$$T = \frac{1}{2} i_A^2 \frac{dL_A}{d\theta} + \frac{1}{2} i_F^2 \frac{dL_F}{d\theta} + i_A i_F \frac{dL_{AF}}{d\theta} \quad (1)$$

Clearly, for positive developed torque the following equations must be satisfied:

$$\begin{cases} i_A \cdot i_F > 0 \\ \dfrac{dL_{AF}}{d\theta} > 0 \end{cases} \quad (2\text{-a})$$

$$\begin{cases} i_A \cdot i_F < 0 \\ \dfrac{dL_{AF}}{d\theta} < 0 \end{cases} \quad (2\text{-b})$$

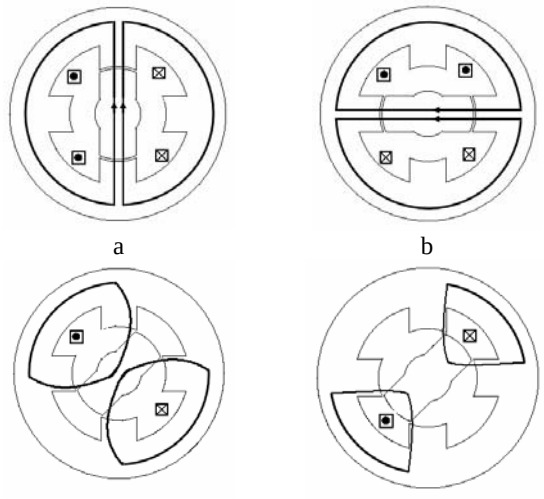

Figure 3: Flux patterns for various excitations and positions

a) Fully aligned position $(\theta = 0, i_F > 0, i_A > 0)$
b) Fully aligned position $(\theta = 90, i_F > 0, i_A < 0)$
c) Fully unaligned position, at which the coupling between field and armature windings is zero $(\theta = 45)$, $i_A = 0$
d) Fully unaligned position $(\theta = 45)$, $i_F = 0$

3. IDEALIZED INDUCTANCES OF FIELD WINDING

A. Self inductance

Figure 4 shows the flux pattern after the excitation of field winding. When the rotor is in the aligned position with the stator poles, the flux goes through stator pole, air gap, rotor pole, and rotor yoke (figure 4-a). As the rotor begins to rotate the overlapped area between stator and rotor poles remains constant up to θ_1. The overlapped area $(a_1(\theta))$, decreases linearly with θ after $\theta = \theta_1$, where $\theta_1 = (\alpha_r - \alpha_s)/2$ (figure 4-b).

Area a_1 becomes zero at $\theta = 180/P_s + \theta_2$, and $\theta_2 = (\alpha_r + \alpha_s - 360/P_s)/2$. As the overlapped area of one rotor pole tip-pair $(a_1(\theta))$ decreases, the overlapped area in the other tip-pair $(a_2(\theta))$ increases. Thus a new path for flux through a_2 expands (figure 4-c). It should be noted that a third area for flux path $(a_3(\theta))$ may exist around $\theta = 180/P_s$. Area a_3 is produced when a_1 and a_2 are not simultaneously equal to zero.

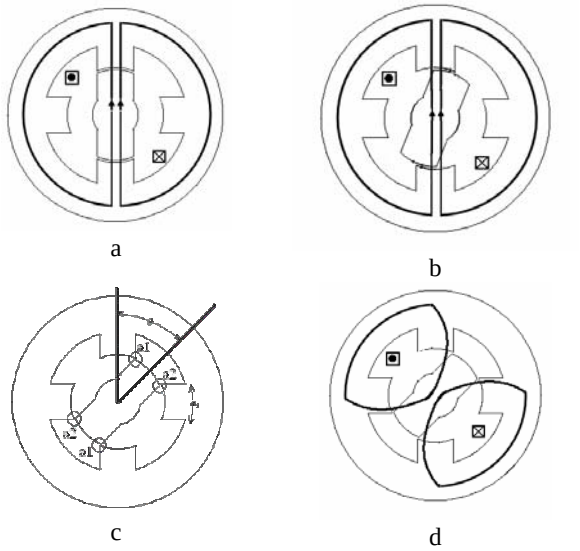

Figure 4: Flux patterns with the field winding excited

Figure 5 shows the profile of the explained areas.

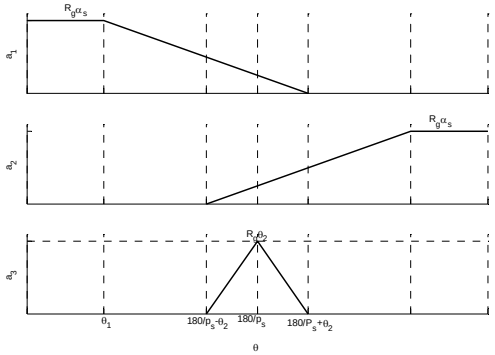

Figure 5: The areas of flux crossings in various paths

To solve for the field intensity, Ampere's law is integrated around a closed contour in figure 6, such as the one which passes through the centers of overlapping poles, air-gaps, and the yoke. The field quantities in the poles along this path are considered as the main field quantities and are denoted with an "*m*" subscript. Equation (3) expresses the integral of Ampere's law around this closed contour. Here, the idealizing assumption is just to neglect the saturation of cores.

$$H_{Fe,m} \cdot 2 \cdot l + H_{g,m} \cdot 2 \cdot g = N_F \cdot I_F \tag{3}$$

Ampere's law can also be integrated around the parallel closed contour in figure 6 where the stator and rotor poles do not overlap. The field quantities along this path are called the fringing field quantities and denoted with an "f" subscript. So:

$$H_{Fe,f1} \cdot 2 \cdot l + H_{g,f1} \cdot 2 \cdot g_{f1} = N_F \cdot I_F \tag{4}$$

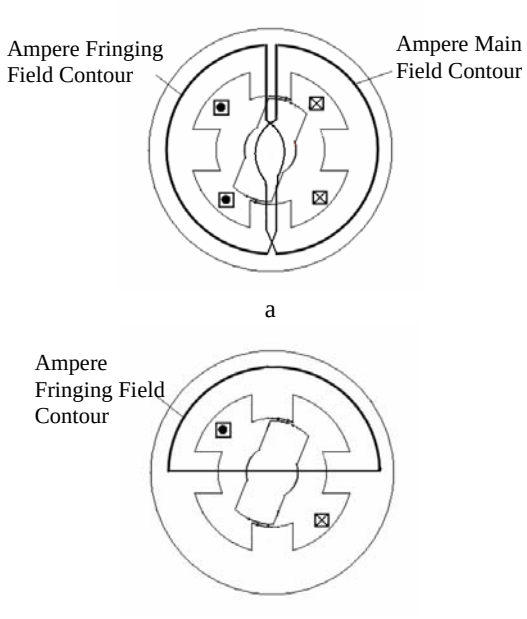

Figure 6: Ampere contours for computing magnetic field

Note that in (4) equivalent air gap (g_{f1}) is applied instead of g and g_{f1} is the length of fringing flux path beyond the stator poles which goes through the air. Another fringing field contour exists in FSM, as shown in figure 6-b. Integrating Ampere's law along this path gives:

$$H_{Fe,f2} \cdot 2 \cdot l + H_{g,f2} \cdot 2 \cdot g_{f2} = N_F \cdot I_F \tag{5}$$

The flux density B, of the pole-shoe is equal to the B field in the air-gap for the main flux solution since the cross-sectional area for the main flux is taken to be constant right through the pole. This flux density is denoted as B_m. Likewise, the B field in the iron is equal to the B in the air gap for fringing flux solution since the cross-sectional area for the fringing flux is also taken to be constant. This field is denoted B_f. Of course B_m does not equal B_f since the air gaps in two regions are different. To find the B field, the constitutive relationship between B and H, which characterizes the materials, must be known. In the air-gap of the main flux ampere contour we have:

$$B_m = \mu_0 H_{g,m} \tag{6}$$

A similar equation holds for the air-gap along fringing flux contour. In the iron along the main flux contour, considering unsaturated core, the following relation holds:

$$B_m = \mu H_{Fe,m} \tag{7}$$

A similar equation holds for the iron along the fringing flux contour. Equations (3), (6), and (7) constitute the equations for the three unknowns $H_{Fe,m}$, $H_{g,m}$ and B_m. One can easily solve for B_m by solving for $H_{g,m}$ from (6), using the result to eliminate $H_{g,m}$ from (3) to get (9), solving (9) for $H_{Fe,m}$, and substituting the result into (7) as in the following:

$$H_{g,m} = \frac{B_m}{\mu_0} \tag{8}$$

$$H_{Fe,m} \cdot l + \frac{B_m}{\mu_0} \cdot g = \frac{1}{2} N_F I_F \tag{9}$$

$$H_{Fe,m} = \frac{N_F I_F}{2l} - \frac{g}{l} \cdot \frac{B_m}{\mu_0} \tag{10}$$

$$B_m = \mu \cdot \left(\frac{1}{l + \mu_r \cdot g} \cdot \frac{N_F I_F}{2} \right) \tag{11}$$

The main flux-linkages of the field winding per stack length is taken to be equal to the area of rotor-stator poles overlap times the number of turns around pole (figure 7) as follows:

$$\lambda_{mF}(\theta, I_F) = N_F \cdot l_{stk} \cdot a_s(\theta) \cdot B_m = \frac{\mu \cdot l_{stk}}{l + \mu_r \cdot g} \cdot a_s(\theta) \cdot \frac{N_F^2 I_F}{2} \tag{12}$$

where, the area of rotor and stator poles overlap $a_s(\theta)$, is equal to $a_1(\theta) + a_2(\theta)$ as shown in figure 7. The fringing flux-linkages of the field winding is:

$$\lambda_{fF}(\theta, I_F) = \mu \cdot \left(\frac{a_{g1}(\theta)}{l + \mu_r \cdot g_{f1}(\theta)} + \frac{a_{g2}(\theta)}{l + \mu_r \cdot g_{f2}(\theta)} \right) \cdot \frac{N_F^2 I_F}{2} \tag{13}$$

where, $a_{g1}(\theta)$ and $a_{g2}(\theta)$ are the fringing flux areas (figure 8), and at full-aligned position $a_{g1}(\theta)$ is approximately equal to:

$$a_{g1}(\theta) = (\alpha_s \cdot R_g + g) \cdot (l_{stk} + g) / l_{stk} - \alpha_s \cdot R_g \tag{14}$$

All quantities on the right hand sides of (12) and (13) are known, except for $g_{f1/2}(\theta)$.

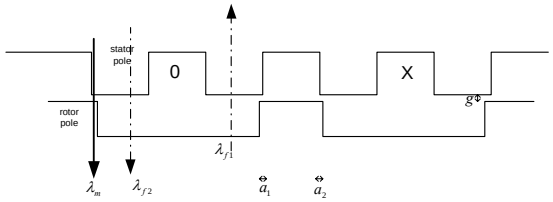

Figure 7: Simplified model to calculate the flux-linkages of the field winding

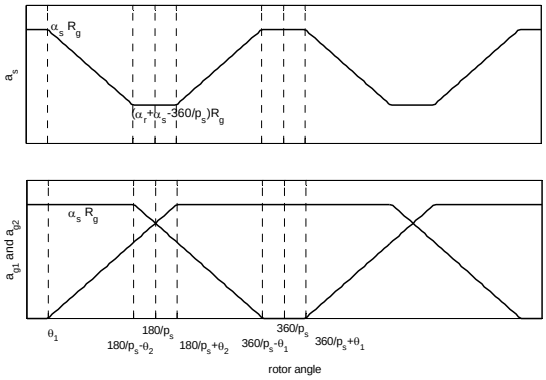

Figure 8: The crossing areas of the main and fringing fluxes

A proposed method to compute $g_{f1,2}(\theta)$ is to define the fringing flux to be the total flux not accounted for by the main flux. This idea is illustrated in figure 9. By calculating the fringing flux-linkages using figure 7 and setting it equal to the one obtained by using figure 9 and knowing that $g_{f1}(180/P_s) = g_{f2}(180/P_s)$ results into the following:

$$\lambda_{fF} = N_F \cdot \left(\frac{360}{p_s} + \alpha_s\right) \cdot R_g \cdot l_{stk} \cdot \frac{N_F I_F}{2} \cdot \frac{\mu_0}{g_0} = N_F \cdot \left(a_{g1}(180/P_s) + a_{g2}(180/P_s)\right) \cdot l_{stk} \cdot \frac{N_F I_F}{2} \cdot \frac{\mu_0}{g_{f1}(180/P_s)} \quad (15)$$

By Solving (15) for $g_{f1}(\theta)$, one obtains:

$$g_{f1}(180/P_s) = \frac{a_{g1}(180/P_s)}{a} \cdot g_0 \quad (16)$$

$g_{f1}(\theta)$ will increase as the $a_{g1}(\theta)$ increases and thus, $g_{f1}(\theta)$ can be approximated as follows:

$$g_{f1}(\theta) = \frac{a_{g1}(\theta)}{a} \cdot g_0 + g \quad (17)$$

Similarly,

$$g_{f2}(\theta) = \frac{a_{g2}(\theta)}{a} \cdot g_0 + g \quad (18)$$

The stator and rotor poles are approximated in figure 9. Therefore to refine the results and to consider the effect of real air gap, the real air gap is added to equations 17 and 18. where,

$$a = (360/P_s + \alpha_s) \cdot R_g \quad (19)$$

g_0 is chosen as such to obtain the required value of inductance L_0 in figure 9. Detailed calculations of g_0 and L_0 are in the appendix.

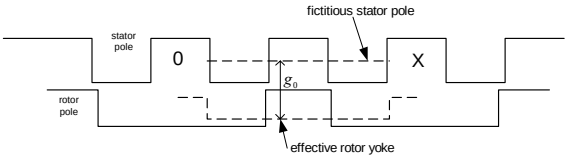

Figure 9: Effective geometry

The total flux-linkages of the field winding due to field current is the summation of λ_{mF} and λ_{fF} multiplied by two, to account for the other leg of the winding:

$$\lambda_F(\theta, I_F) = 2 \cdot (\lambda_{mF}(\theta, I_F) + \lambda_{fF}(\theta, I_F)) \quad (20)$$

Now, the self inductance of the field winding is obtained as follows:

$$L_F(\theta) = \frac{\lambda_F(\theta, I_F)}{I_F} = \left(\frac{1}{l + \mu_r \cdot g} \cdot a_s(\theta) + \frac{1}{l + \mu_r \cdot g_{f1}(\theta)} \cdot a_{g1}(\theta) + \frac{1}{l + \mu_r \cdot g_{f2}(\theta)} \cdot a_{g2}(\theta)\right) \cdot \mu \cdot l_{stk} \cdot N_F^2 \quad (21)$$

Because of symmetry, the self-inductance of the armature winding can also be expressed as in the following:

$$L_A(\theta) = L_F(\theta - 360/P_s) \quad (22)$$

B. Mutual inductance

Again, it is assumed without loss of generality, that only the field winding is excited. The other assumptions are as before.

In order to obtain the mutual inductance three issues should be considered carefully. The First one is that the fringing component of flux does not contribute mutual inductance. The second point is that when $a_1(\theta)$ and $a_2(\theta)$ are not both equal to zero, the flux of the field winding does not go through the armature winding (figure 4-d). The third one is that after passing the unaligned position, the flux will switch between poles, so that in this region the polarity of the induced electro-motive-force will change.

According to figure 10, the effective area of the stator-rotor-poles overlap is $a_m(\theta) = a_1(\theta) - a_2(\theta)$. And hence, the mutual flux linkage between the field and armature windings is as in the following:

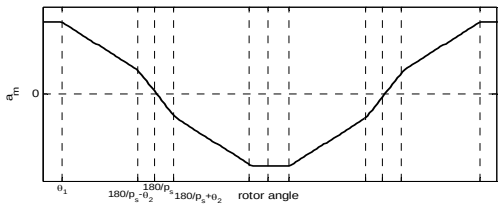

Figure 10: The effective area to calculate the mutual inductance L_{AF}.

$$\lambda_{AF}(\theta, I_F) = N_A \cdot a_m(\theta) \cdot l_{stk} \cdot B_m = \frac{\mu \cdot l_{stk}}{l + \mu_r \cdot g} \cdot a_m(\theta) \cdot N_A N_F \cdot I_F \quad (23)$$

And the mutual inductance is:

$$L_{AF}(\theta) = \frac{\lambda_{AF}(\theta, I_F)}{I_F} = \frac{\mu \cdot l_{stk}}{l + \mu_r \cdot g} \cdot a_m(\theta) \cdot N_A N_F \quad (24)$$

4. RESULTS

The proposed analytic approach is applied to model an FSM with the dimensions given in table 1. As it can be seen from figure 11, the self and mutual inductance profiles are very similar to the idealized inductance profile of figure 2. It is observed from figure 12 that the proposed model predicts the mutual inductance very accurately within 5% of the 2-D finite element method.

TABLE 1: THE DIMENSIONS OF THE MODELED MOTOR

Specifications	Type I	Type II
Stator-pole arc (degrees)	45	45
Rotor-pole arc (degrees)	60	45
Stator-pole height (mm)	50	50
Rotor-pole height (mm)	30	30
Air-gap (mm)	5	0.5
Number of field-coil turns	100	100
Number of armature-coil turns	100	100
Rotor radius (mm)	100	100
Stator-yoke height (mm)	80	80
Number of stator/rotor poles	4/2	4/2

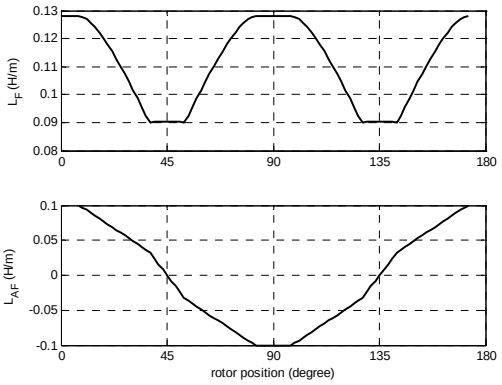

Figure 11: The inductance profiles obtained by the proposed method (for motor type I)

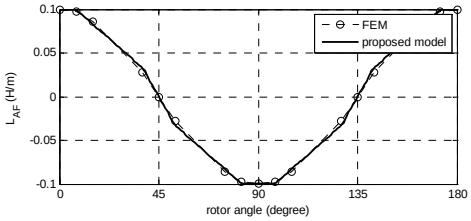

Figure 12: The mutual-inductance profile obtained by the proposed model and FEM (for motor type I)

Although the proposed model predicts the mutual inductance accurately, the prediction of self-inductance in the unaligned position of rotor is not as accurate. Figure 13 displays the predicted self-inductance and its comparison with the FEM results.

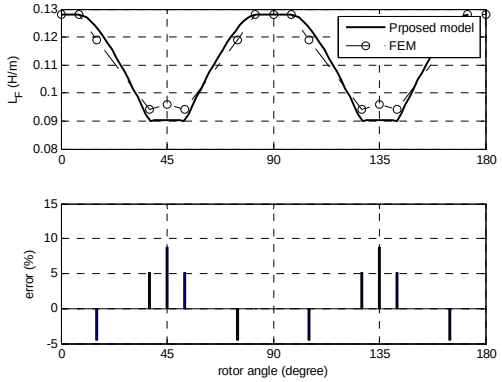

Figure 13: The self-inductance obtained by the proposed model and FEM, and the prediction errors (for motor type I)

The maximum error of predictions is 10% which happens at the unaligned position. The authors believe that the source of these errors might be in the calculation of area for the fringing flux.

The proposed model has also been implemented to model motor type II with the specifications summarized in table 1. Figure 14 shows the results.

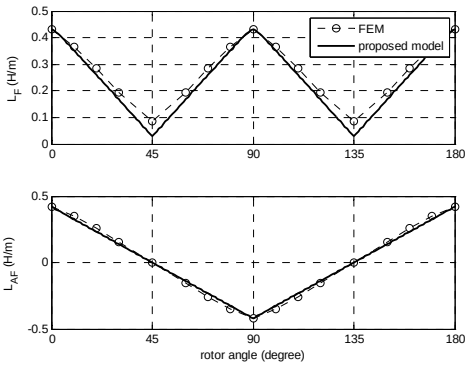

Figure 14: The self- and mutual-inductances obtained by the proposed model and FEM (for motor type II)

Again the proposed model can calculate mutual inductance accurately, but it is not as accurate in predicting the self-inductance in the unaligned position at 45^0.

5. CONCLUSION

An analytical approach to model flux switching motors has been described. The proposed model is correct if a piece-wise saturation of core is assumed. As it is deduced from figures 12 and 14, the proposed method predicts the mutual inductance accurately with a maximum error of 5%. However, the proposed model is not as accurate in the calculation of the self-inductance. The error is within 10% of the finite element method. The authors are now working to see if the area for the fringing flux can be obtained more accurately.

6. APPENDIX

An analytic solution for the unaligned inductance will be obtained by following the classical procedure for the 2-D field. The main equations are the magnetostatic Maxwell's equations.

$$\nabla \times \vec{A} = \vec{B} \qquad \text{A-1}$$

$$\nabla \cdot \vec{A} = 0 \qquad \text{A-2}$$

$$\nabla^2 \vec{A} = -\mu \cdot \vec{J} \qquad \text{A-3}$$

It is well known that for a 2-D problem, where the current flows only in *z* direction, only the *z* component of the vector potential is nonzero hence:

$$\nabla^2 A_z = -\mu \cdot J_z \qquad \text{A-4}$$

The geometry of problem is approximated by a rectangle as shown in figure A-1.

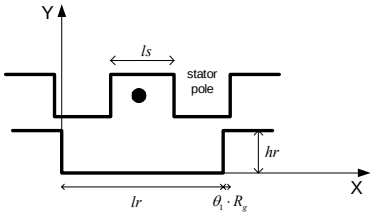

Figure A-1: Rectangular geometry to obtain field

There is no current in the rotor slot so that the right-hand side of (A-4) in this area is zero, and hence we will have the Laplace's equation. In figure (A-1) much of the box is bounded by iron so that, with the assumption of zero $\vec{H}$ field in the iron, the boundary condition on the boundary of box where there is iron is that the tangential $\vec{H}$ field is zero. Thus, the *y* and *x* components of $\vec{H}$ are zero on the two vertical boundaries and on the lower edge of box, respectively. To obtain an approximated value for the *x* component of $\vec{H}$ at $y = hr$ where there is no iron, it will be assumed that the *x* directed field is constant. In this case the integral form of Ampere's law can be used to find this constant value as:

$$H_x(x, hr) = \frac{NI}{ls} \qquad \text{A-5}$$

The solution to Laplace's equation inside of a rectangular box is known and can be written as:

$$Azr = \sum_{n=1}^{\infty} Ar_n \cdot \cosh\left(\frac{\pi n y}{lr}\right) \cdot \cos\left(\frac{\pi n x}{lr}\right) \qquad \text{A-6}$$

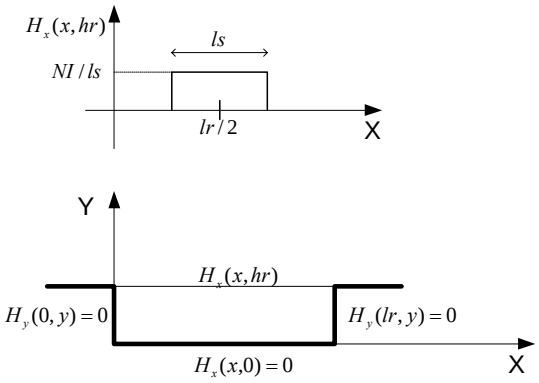

Figure A-2: boundary conditions on the periphery of rectangle.

The $\vec{H}$ is found by taking the curl of the vector potential and dividing it by μ_0.

$$\vec{Hr}(x, y) = \sum_{n=1}^{\infty} Ar_n \cdot \frac{\pi n}{\mu_0 lr} \cdot \{\hat{i}_x \cdot \sinh\left(\frac{\pi n y}{lr}\right) \cdot \cos\left(\frac{\pi n x}{lr}\right) + \hat{i}_x \cdot \cosh\left(\frac{\pi n y}{lr}\right) \cdot \sin\left(\frac{\pi n x}{lr}\right)\} \qquad \text{A-7}$$

The $\vec{H}$ field in (A-7) satisfies all of the boundary conditions except the one at $y = hr$. This boundary condition determines Ar_n. An expansion of $\vec{H}$ in

Fourier series is:

$$H_x(x, hr) = \sum_{n=1}^{\infty} a_n \cdot \cos\left(\frac{\pi n x}{lr}\right) \quad \text{A-8}$$

where a_n is:

$$a_n = \frac{2NI}{\pi n} \cdot \left\{\cos\left(\frac{\pi n}{2}\right) \cdot \sin\left(\frac{\pi n \cdot ls}{2lr}\right)\right\} \quad \text{A-9}$$

Evaluating (A-7) at $y = hr$, and setting it equal to (A-8) gives the following:

$$Ar_n = \frac{2 \cdot \mu_0 \cdot lr \cdot NI}{(\pi n)^2} \cdot \frac{\cos\left(\frac{\pi n}{2}\right) \cdot \sin\left(\frac{\pi n \cdot ls}{2lr}\right)}{\sinh\left(\frac{\pi n \cdot hr}{lr}\right)} \quad \text{A-10}$$

Substituting (A-10) into (A-7) and multiplying the result by μ_0 gives the flux density components as:

$$\bar{B}r_x(x, y) = \sum_{n:even}^{\infty} \frac{2 \cdot \mu_0 \cdot NI}{\pi n} \cdot \frac{\cos\left(\frac{\pi n}{2}\right) \cdot \sin\left(\frac{\pi n \cdot ls}{2lr}\right)}{\sinh\left(\frac{\pi n \cdot hr}{lr}\right)} \cdot \sinh\left(\frac{\pi n y}{lr}\right) \cdot \cos\left(\frac{\pi n x}{lr}\right) \quad \text{A-11}$$

$$\bar{B}r_y(x, y) = \sum_{n:even}^{\infty} \frac{2 \cdot \mu_0 \cdot NI}{\pi n} \cdot \frac{\cos\left(\frac{\pi n}{2}\right) \cdot \sin\left(\frac{\pi n \cdot ls}{2lr}\right)}{\sinh\left(\frac{\pi n \cdot hr}{lr}\right)} \cdot \cosh\left(\frac{\pi n y}{lr}\right) \cdot \sin\left(\frac{\pi n x}{lr}\right) \quad \text{A-12}$$

Integrating B over the surface enclosed by winding from left tip of rotor slot to the middle of slot i.e. $x = 0 \rightarrow lr/2$ and along the stack gives the flux linkage of rotor slot. The normal of this surface is in the y direction so that only y - directed component of B at $y = hr$ should be integrated. Due to the other leg of winding, the result should be multiplied by two.

$$\lambda_{rs} = 2 \cdot N \cdot l_{stk} \int_0^{lr/2} Br_y(x, hr) \cdot dx = 4\mu_0 \cdot N^2 \cdot l_{stk} \cdot l_r \cdot \sum_{n:even} \frac{\sin\left(\frac{\pi n \cdot ls}{2lr}\right)}{(\pi n)^2 \cdot \tanh\left(\frac{\pi n \cdot hr}{lr}\right)} \cdot ((-1)^{n/2} - 1) \cdot I \quad \text{A-13}$$

Dividing (A-13) by the current gives the rotor slot contribution to the inductance.

$$L_{rs} = 4\mu_0 \cdot N^2 \cdot l_{stk} \cdot l_r \cdot \sum_{n:even} \frac{\sin\left(\frac{\pi n \cdot ls}{2lr}\right)}{(\pi n)^2 \cdot \tanh\left(\frac{\pi n \cdot hr}{lr}\right)} \cdot ((-1)^{n/2} - 1) \quad \text{A-14}$$

The rotor pole contribution to inductance can be obtained easily by considering an ideal core as:

$$L_{rp} = 2 \cdot \mu_0 \cdot R_g \theta_1 \cdot l_{stk} \cdot N^2 / (2g) \quad \text{A-15}$$

The inductance at the unaligned position becomes:

$$L_0 = 2 \cdot (L_{rs} + L_{rp}) \quad \text{A-16}$$

In figure 9, g_0 is chosen such that the required value of inductance L_0 is obtained as in the following:

$$g_0 = \mu_0 \cdot a \cdot N^2 / (2L_0) \quad \text{A-17}$$

where $a = (360 / P_s + \alpha_s) \cdot R_g$.

7. REFERENCES

[1] Pollock, C.; Wallace, M.; "The flux switching motor, a DC motor without magnets or brushes", Thirty-Fourth IAS Annual Meeting. Industry Applications Conference, 1999. Conference Record of the 1999 IEEE Volume 3, 3-7 Oct. 1999 Page(s):1980 - 1987 vol.3

[2] Pollock, C.; Brackley, M.; "Comparison of the acoustic noise of a flux-switching and a switched reluctance drive", IEEE Transactions on Industry Applications, Volume 39, Issue 3, May-June 2003 Page(s):826 - 834

[3] Reeve, J.M.; Pollock, C.; "Dynamic simulation model for two-phase mutually coupled reluctance machines', Thirty-Sixth IAS Annual Meeting. Record of the 2001 IEEE Conference Industry Applications Conference, 2001. Volume 1, 30 Sept.-4 Oct. 2001 Page(s):40 - 47 vol.1

[4] Pollock, C.; Pollock, H.; Barron, R.; Coles, J.R.; Moule, D.; "Court, A.; Sutton, R.; Flux-Switching Motors for Automotive Applications", IEEE Transactions on Industry Applications, Volume 42, Issue 5, Sept.-Oct. 2006 Page(s):1177 - 1184

[5] S. E. Abdollahi, M. Mirsalim, M Mirzayee, M. Ehsani, and S. Gay, "Two-dimensional finite element and analytical modelling of a solid rotor disk induction motor", International Scientific Quarterly 'ELECTROMOTION' (ISSN 1223 – 057X), Vol. 10, No. 3, 2003

[6] M. Mirzaei, M. Mirsalim (IEEE Senior Member) , and E. Abdollahi, "Analytical Modeling of Axial Air-Gap Solid Rotor Induction Machines Using a Quasi-Three-Dimensional Method", IEEE TRANSACTIONS ON MAGNETICS, VOL.43, NO.7, July 2007.

[7] M. Mardaneh, M. Mirsalim, M. AliAhmadi, "A New Approach in Modelling and Design of Axial-Flux Permanent Magnet Machines", Amirkabir Journal of Science and Technology.

[8] T. J. E. Miller, "Nonliner Theory of the Switched Reluctance Motor for Rapid Computer-aided Design", IEE PROCEEDINGS, Vol. 137, November 1990.

[9] Hossain, S.A.; Husain, I., "A geometry based simplified analytical model of switched reluctance machines for real-time controller implementation", Power Electronics, IEEE Transactions on Volume 18, Issue 6, Nov. 2003.

[10] Suzuki, T.; Tereda, M.; et.al. "A rotor angular position estimation based on a simple mathematical expression of the magnetizing characteristics of switched reluctance machines", IEEE 2005

[11] Arthur Radun, "Analytically computing the flux linked by a switched reluctance motor phase when the stator and rotor poles overlap", IEEE Transaction on Magnetics, Vol. 36, No. 4, July 2000, pp. 1996-2003.

[12] Hossain, S.A.; Husain, I.; "A geometry based simplified analytical model of switched reluctance machines for real-time controller implementation", Power Electronics Specialists Conference, 2002. pesc 02. 2002 IEEE 33rd Annual, Page(s): 839 - 844 vol.2.

[13] R. Krishnan "Switched Reluctance Motor Drives: Modeling, Simulation, Analysis, Design, and Applications", ISBN: 0849308380 Pub. Date: June 2001, publisher: CRC Press.

[14] T. Lachman, T.R. Mohamad, C.H.Fong, "Nonlinear modeling of switched reluctance motors using artificial intelligence techniques", IEE Proc. Electr. Power Application, Vol. 151, No. 1, January 2004, page(s): 53- 60.